Journal of Biomechanics 162 (2024) 111858

Contents lists available at ScienceDirect

Journal of Biomechanics

journal homepage: www.elsevier.com/locate/jbiomech

Design and optimisation of an Intra-Aortic Shrouded rotor axial pump

Elif Oran [a], Essam Abo-Serie [b,*], James Jewkes [b], Manus Henry [a,c], Bulent Oran [d]

[a] Coventry University, Centre for Fluid and Complex Systems, Coventry, UK
[b] University of Leicester, School of Engineering, Leicester, UK
[c] University of Oxford, Department of Engineering Science, Oxford, UK
[d] Medicana International Hospital, Department of Pediatric Cardiology, Izmir, Turkey

ARTICLE INFO

Keywords:
Ventricular assist device
Minimally invasive heart assist pump
Mechanical circulatory assistance
Pediatric circulatory support
Rotary blood pump

ABSTRACT

Undesirable side effects in patients with a LVAD (Left Ventricular Assist Device) pump fitted include blood damage, thrombosis, blood traumatisation, and End-Organ Disfunctions. These side effects have generally been attributed to the high wall shear stresses and the induced turbulent flow. In this study, we introduce a novel design to address these effects by lowering the rotational speed and providing an optimum flow path design to minimise blood damage. We present an initial scheme for a new Intra-Aortic Shrouded Rotary Axial Pump and develop a sequence of pump geometries, for which the Taguchi Design Optimisation Method has been applied. We apply CFD tools to simulate the pressure rise, pump performance, hydraulic efficiency, wall shear stress, exposure time and mass flow rate. A prototype pump has been tested in a mock cardiovascular circuit using a water-glycerol solution. The optimum design delivered the desired pressure/mass flow rate characteristics at a significantly low rpm (2900 rpm). As a result, the estimated blood damage index is low, matching the design requirements. The theoretical performance was matched by experimental results.

1. Introduction

Diagnosed heart failure incidence has been increasing, with over 1 million new cases worldwide annually. The number of available donor organs cannot meet the growing demand (Chen et al., 2018). Survival rates of patients using LVADs for 1 year and 2 years are 85% and 75%, respectively (Starling et al., 2011). Despite the remarkable survival rates, the success of LVAD therapy has not been clinically accepted, due to significant adverse events. Furthermore, these survival rates are insufficient when considering the expected delay for heart transplantation. The number of patients on a waiting list far exceed the number of heart donors in the UK (Messer et al., 2019), with similar imbalances observed internationally.

Moreover, the necessity for LVADs increases day by day. Currently, heart transplantation offers better long-term survival rates for patients with end-stage heart failure, but the selection criteria for suitable patients are very narrow, considering multiple factors including age, prior operation history, end-organ function and appropriate health insurance coverage (Chen et al., 2018). Thus, a growing group of patients are not suitable for heart transplantation. An alternative is to provide durable LVADs, and this is considered to be the only option for those who cannot meet the criteria for heart transplantation (Al-Naamani et al., 2021). It is well-known that approximately 50% of patients diagnosed with heart failure will not survive more than 5 years. There is no doubt that LVADs need to be enhanced further. Heart disease is still the main cause of mortality globally, primarily due to extended lifespans in developed countries. Near term improvements in current LVADs designs may be insufficient to overcome the side effects caused by their inherent design limitations requiring a high rotation speed and/or a high blood contact area.

However, over the last five years, a number of innovative LVADs have been developed and implanted in patients. Advances in LVAD pump design have enabled the evolution of new surgical techniques using less invasive procedures. New intra-pericardial LVADs, developed by Thorotec (HM3) and HeartWare (HVAD), have no inflow cannula (Carrozzini et al., 2019). With these devices, the artificial vessel size has been reduced, and a new minimally invasive implementation technique has been developed that reduces surgical trauma (Rogers et al., 2012). As a result of this technique, less hemodialysis, fewer blood transfusions and significantly reduced intensive-care unit and hospital stays are observed (Al-Naamani et al., 2021). The introduction of the new generation of intra-pericardial centrifugal pumps has been accompanied by

* Corresponding author at: University of Leicester, School of Engineering, University Rd, Leicester LE1 7RH, UK.
E-mail address: e.aboserie@leicester.ac.uk (E. Abo-Serie).

https://doi.org/10.1016/j.jbiomech.2023.111858
Accepted 1 November 2023
Available online 4 November 2023

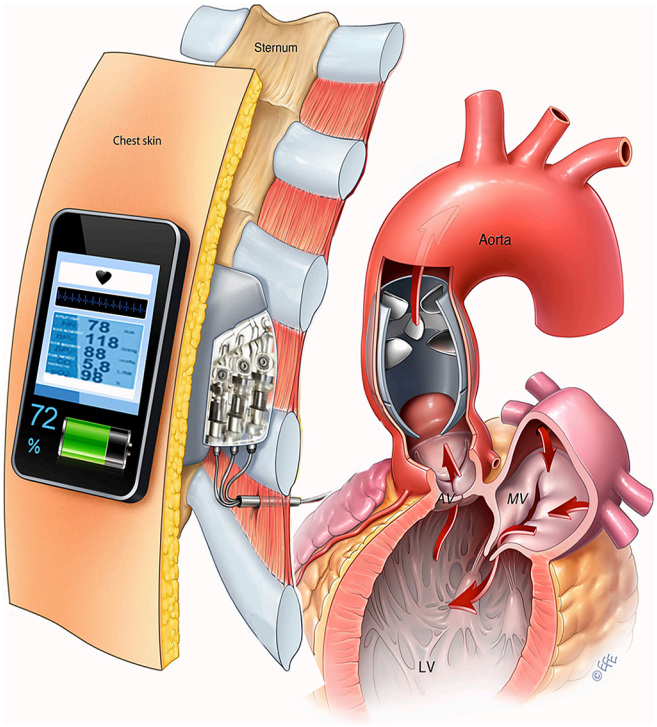

Fig. 1. The proposed design VAD with a magnetically levitated axial pump rotor located in the aorta to be powered via a wirelessly charged battery inside the body.

the emergence of alternative minimal invasive surgical procedures that lower the surgical trauma and may maximise postoperative survival rates. Decreasing the blood contact surface and the size of invasive procedure play a key role in lowering the hospital stay and hemodialysis. However, the survival rate is still unacceptably low, with the main reasons for morbidities being stroke, pump thrombosis and bleeding (Benjamin et al., 2017; Netuka et al., 2017; Fang et al., 2015; Fuchs et al., 2019; Vasudevan et al., 2019; Topkara et al., 2016).

According to research conducted on 342 patients with LVAD in the UK, the 30-day survival rate after LVAD implantation was 88.9%, whereas the overall patient survival rate within 3 years after having LVAD implant was only 49.6%. (Parameshwar et al., 2019) Of these 342 patients, 61 were added to the urgent list for heart transplantation. The leading reasons for urgent listing were pump thrombosis, device-related complications including life-threatening infection, and mechanical failures. 85 of those 342 patients (24.8%) received a heart transplant during the research period. Artificial surfaces in these rotary pump devices and inherently high mechanical shear stresses are considered to be the main factors for blood trauma which can cause hemostatic and hematological complications in patients with LVAD (Slaughter et al., 2010). To avoid these drawbacks, the new generation of intrapericardial pumps are developing the further innovative solutions required, since heart failure (HF) is one of the largest unsolved problems in cardiac care today (Chen et al. 2018). The survival rate that is reached today is an emergency call to develop further new generation innovative LVADs when we consider the increase of one million new cases each year (Mehra, et al., 2018; Stawiarski and Ramakrishna, 2021; Nassif et al., 2021). Future developments should aim to further minimise invasive procedures and the hemolysis problem. Here we propose an innovative intra-aortic LVAD that is implanted without any surgical cut on the heart itself and placed inside the aorta to assist the heart without requiring any artificial blood vessels.

In this study, we present the initial design of an innovative intra-aortic LVAD that is placed inside the aorta (Fig. 1). We start with an initial design determined by anatomic size constraints. Iterative designs are developed to improve the geometrical characteristics of the pump by applying the Taguchi Design Optimisation Method (TDOM).

After determining the design characteristics, we employ computational fluid dynamics (CFD) studies to identify the optimal designs and assess the pump geometries. Then, we investigate pressure rise, pump performance, hydraulic efficiency, wall shear stress levels and blood damage index to optimise the new design for minimal hemolysis and thrombosis. This innovative pump has potential as a solution for stroke and bleeding events. Prototypes of the pump have been manufactured and tested in a mock cardiovascular circuit using a water-glycerin blood analogue solution.

2. Materials and methods

2.1. Intra-Aortic design requirements

Considering the minimal invasive procedure requirements, a new pump was predesigned to be implantable in the aorta (Fig. 1) (Oran and Oran, 2017). The aim of this intra-aortic pump is to assist the heart as a LVAD device, and to negate the need for any cut on the heart itself. Furthermore, in this proposed design, there is no need for any artificial vessels, and the shaftless impeller design provides blood flow without creating a narrowed vessel that is detrimental to human health. With the new design, even if the device stops running, there is no blockage for the aorta (Fig. 1). The intra-aortic pump device contrasts with the current generation of devices that bypass the heart, giving rise to potential harm to the heart itself.

Given its location in the aorta, the design requirements differ substantially from current LVADs. Current devices are designed to accept 0 mm-Hg inlet pressure and deliver 120 mm-Hg outlet pressure. Since these devices receive flow from the ventricle, they use the zero ventricular pressure as the input pressure. The proposed pump will be located in the aorta which experiences a pressure variation from 80 to 120 mmHg during the cardiac cycle (Dewi and Yusof, 2020and Yousof; Mori et al., 2019; Guyton, 1973). Accordingly, the inlet pressure is set at the minimum value of 80 mmHg in this study. The pump will reduce the overall pressure required from the heart as it will sympathetically and dynamically support its cardiac cycle.

The required pressure difference produced by LVADs is 120 mm-Hg because they are connected in parallel to the heart via artificial vessels. Thus, the pressure difference they must deliver is approximately 100–120 mm-Hg. By contrast, the new LVAD only delivers a 40 mm-Hg pressure difference, while performing the same task as other devices that produce three times the pressure head. This advantage arises from the intra-aortic placement of the device which ensures a minimum value of 80 mmHg as the input pressure. Since it is placed in series with the heart, the pressure difference it must generate is only 40 mmHg. The function of LVADs is to support or replace the pumping function of the heart's left ventricle. A typical operating requirement is to pump 5 L/min at a minimum of 100 mmHg aortic pressure (Behbahani et al., 2009). Generating 5 L/min at 40 mmHg pressure head is enough for our proposed LVAD to reach 120 mmHg aortic pressure because of its intra-aortic placement.

The device should be designed to match the anatomy of the aorta. The mean diameter of ascending aorta reported by (Sedghi et al., 2019) was 33.9 $\pm$ 3.3 mm for females and 36.7 $\pm$ 3.5 mm for males. Similar values are reported by Kälsch et al. (2013) and Wolak et al. (2008). The outer diameter of the new design should match these values, and a suitable diameter for the flow path is about 30 mm. However, the flow path diameter of classic LVAD pumps varies between 8 and 15 mm. The positioning of these devices in the body does not allow larger diameters. Rotation speeds for classic axial LVADs are 8000–18000 rpm. In the new LVAD, larger flow path diameters reduce the rotation speed, which in turn may reduce blood trauma.

Table 1
Intra-aortic pump design parameters and value ranges.

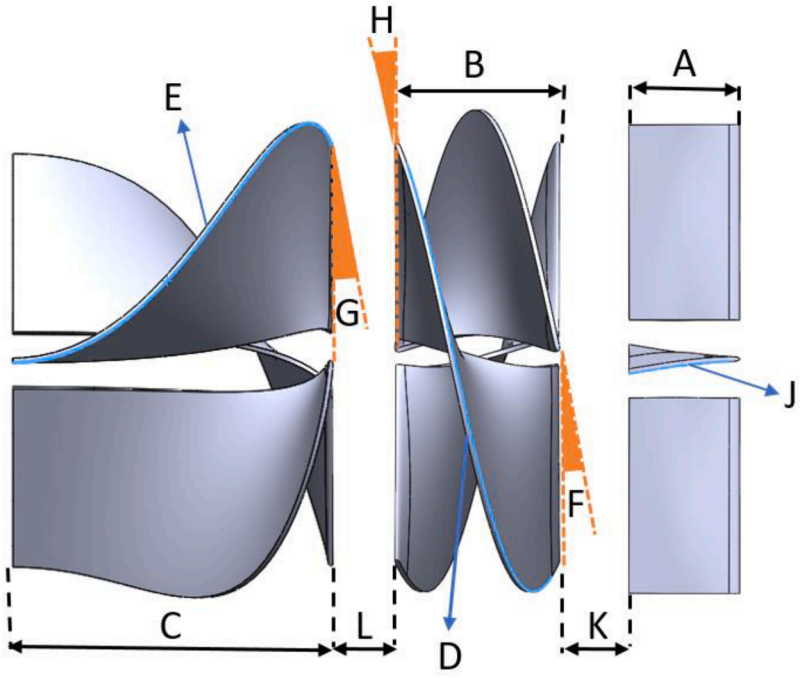

	Optimization Parameters	Values of parameters
A	length of straightener blades (mm)	5, 8, 11
B	length of rotor blades (mm)	10, 15, 20
C	length of diffuser blades (mm)	10, 15, 20
D	wrap angle of rotor (degree)	200°, 280°, 360°
E	wrap angle of diffuser (degree)	80°, 120°, 160°
F	inlet angle of rotor (degree)	1°, 2°, 3°
G	inlet angle of diffuser (degree)	1°, 2°, 3°
H	outlet angle of rotor (degree)	1°, 2°, 3°
J	inlet angle of straightener (degree)	0°, 5 °, 10°
K	Distance between rotor and straightener (mm)	1, 2, 3
L	Distance between rotor and diffuser (mm)	1, 2, 3

2.2. Design of the axial intra-aortic LVAD geometry

The impellers of the intra-aortic pump were initially designed (Abo-Serie et al.,2018; Oran and Oran, 2017) using CFturbo software which enables the creation and design of blades from scratch (cfturbo.com). The software develops blade formation by evaluating the effect of multiple parameters together, such as blade angles, wrap angle and the length of the blades, etc. In this study, we conducted TDOM analysis using 3 different values each of eleven critical geometric parameters for the design optimisation process (Table 1), based on an orthogonal design matrix principle (Zhou et al., 2013). The geometric configurations of TDOM analysis results in a matrix of 27 different designs. The impact of each of these design parameter sets is evaluated based on its ability to deliver the required pump performance. The three selected values for each parameter in one column are matched to the other three selected values of the parameters in another column (Singh et al., 2017; Sarkisyan et al., 2021). This matching procedure allowed us to minimise the number of simulations and maximise the data to clarify what the optimum design parameter values are for a superior-performing blade geometry. Furthermore, the signal-to-noise ratio (S/N) of these parameters and values can be calculated. The highest S/N value for a specific performance output is the optimum geometry for this purpose. This specific performance output is defined according to the aim of the optimisation and can be maximum efficiency, lower blood damage etc. (Califano, et al., 2012; Boyle et al., 2014; Burggren et al., 2014; Kirklin et al., 2014; Smith et al., 2018).

In this geometry, there are flow straightener blades at the entrance of the flow path, a shaft-less rotor in the middle, and a diffuser at the outlet of the intra-aortic axial pump. The function of the straightener is to reduce the incidence angle of flow to the leading edge of the rotor blades. The rotor transforms the mechanical rotational energy of the pump into a rise in pressure. The diffuser blades convert flow rotational energy into additional pressure rise. The centre of the pump is empty to provide unrestricted blood flow. The pump is designed to increase pressure by 40 mmHg and provide a flow rate of 5 L per minute. Since it is connected to the heart in series and placed into the aorta, the pump inlet pressure is about 80 mmHg, and the pump outlet pressure is around 120 mmHg in order to reach the required values of a healthy person.

2.3. Computational method

The flow domain for CFD simulation was obtained by filling the volume inside the pump blades and adding cylinders to extend the domain in StarCCM+ software. This domain was divided into 5 sections with 4 interfaces, an inlet and an outlet (Fig. 2). The automated mesh is used together with surface, polyhedral and prism layers to generate the mesh, and a mesh independence study was conducted to determine the appropriate size for simulation. The aim is to generate a superior-quality mesh with sufficient resolution to represent the major elements of the geometry (McElroy et al., 2020). In the final arrangement, the fluid

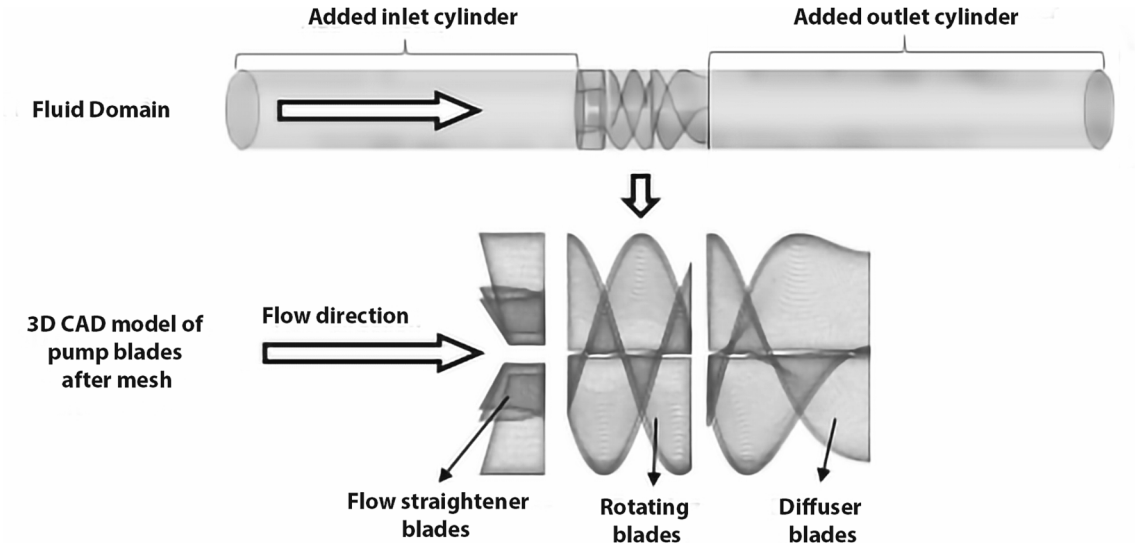

Fig. 2. The CAD model of initial flow domain and meshed blade geometry.

domain is divided into approximately 4 million cells (Fig. 2).

The "k-Epsilon turbulence model" was used in CFD analysis and simulations were carried out for the 27 different designs under the same steady state conditions. Previously published works (Cheng et al, 2021; Fraser et al, 2011) successfully used k-epsilon in their pump simulation. k-omega model is better suited to adverse pressure gradients and separated flow to pick up more accurate flow details in the separated regions (Wilcox, 1998). However, for calculating the equivalent shear stress and the flow at exit which is not highly turbulent k-epsilon is more computationally efficient. In this case the k-epsilon model was found to provide an overall pressure rise value closer to the experimental results.

The fluid was defined as Newtonian with a constant density of 1060 kg m-3 and viscosity of 3.5 × 10–3 Pa s to match the properties of blood (Puhan et al., 2021; Chaichana et al., 2011; Nammakie et al., 2017). A mass flow boundary condition was applied, imposing a uniform velocity at the pipe inlet. At the outlet, a zero gradient boundary condition was applied sufficiently far downstream so as not to influence the region of interest. These boundary conditions allow the pressure rise to be evaluated. A moving reference frame has been used to simulate the rotation (Silva et al., 2021; Khoo et al., 2018). Shear stresses on blades were evaluated, and the torque required to rotate the blades was calculated for each of the 27 geometries.

2.4. *Experimental method*

After optimising the flow path geometry using numerical methods, the optimal axial intra-aortic pump geometries were prototyped. A cardiovascular circulatory loop was built to test the shaft-less blade models (fig-3). This includes a shaftless electric motor framework, where the blades are fixed inside the motor. The aortic pressure level of the cardiac cycle is calculated by the height of the liquid in the acrylic tube. This height also indicates the differential pressure between the inlet and outlet of the pump. During the experiments, the tank was used as over fill and fed continuously by another pump to keep the liquid level

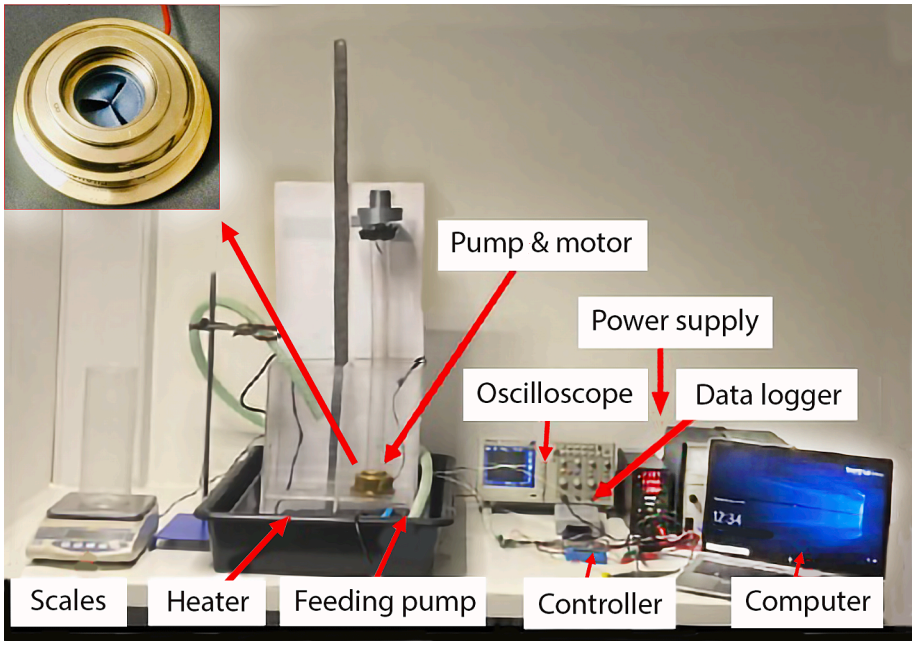

Fig. 3. The cardiovascular test setup.

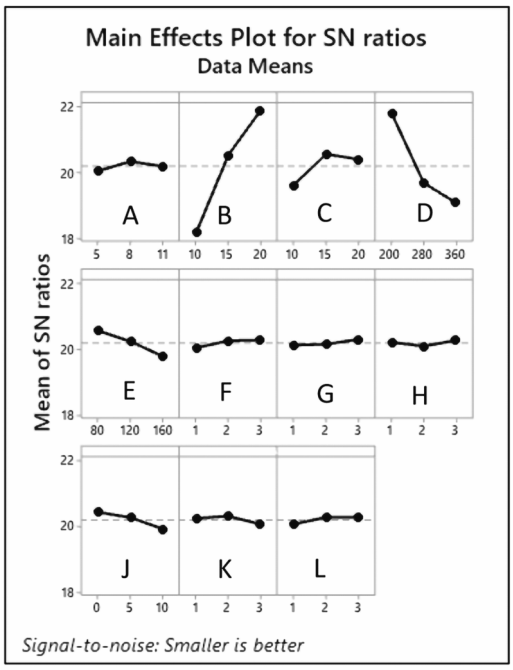

(a)

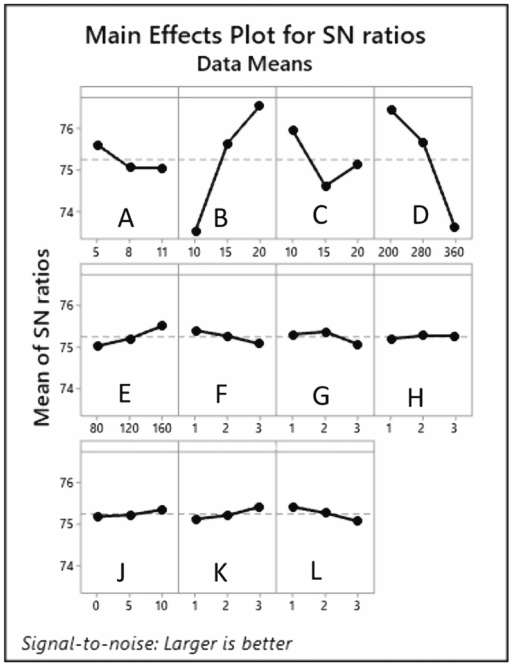

(b)

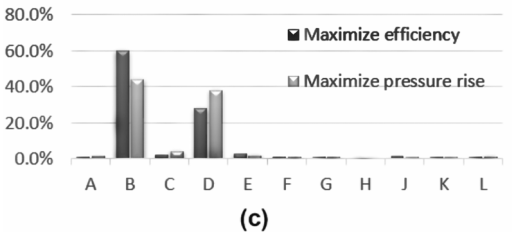

(c)

Fig. 4. Main effects plot of (S/N) ratios for the Taguchi method to maximize efficiency (a) and maximize Pressure rise (b). Bar chart (c) demonstrates the impact percentage of parameters on efficiency and pressure rise.

stable. Additionally, the necessary flow rate can be adjusted by changing pump speed. The prototype was validated utilising a blood analog solution from a mixture of water and glycerol (Vignali et al., 2022; Ribaric and Kordaš, 2011).

The test setup includes a pump prototype with a flow line diameter of 30 mm placed inside the reservoir (See Fig. 3). The fluid is sucked from the pump suction nozzle and moves vertically towards the collection reservoir.

The flow rate was calculated by determining how much liquid is transferred for the duration of the experiment: the liquid collected during the test is transferred to a tared container and weighed. The weight of the accumulated liquid is measured and divided by the experimental time. Two different systems are used to control the experiment and collect data. The first is a data acquisition system, which includes a recording of the experimental temperature. The second system drives the electric motor of the pump using a brushless direct current (BLDC) motor controller. The rotation speed of the motor is stable for steady state conditions and is adjusted via this controller. The pressure difference between the pump inlet and outlet is measured as differential pressure with the height of the liquid in the acrylic tube acting as a basic manometer.

3. Results

3.1. Taguchi design optimisation results

Fig. 4 shows the 27 combinations and their outputs that were performed according to the TDOM analysis. The numerical CFD method is used to calculate the pressure rise and pump efficiency for each combination as outputs. The Signal to Noise (S/N) ratios were calculated to find the most efficient geometry and the geometry that generates the highest pressure rise. Fig. 4 shows the main effects plot of the S/N ratios for pump efficiency of the new intra-aortic pump, and Fig. 4 (b) shows the corresponding results for the pressure rise generated by the pump.

The length of the rotor blades and their wrap angles have a significant impact on both the pressure generation of the rotating blades and the pump efficiency. Longer rotor blades produce maximum pressure while shorter rotor blades play the biggest role in increasing pump efficiency (see Fig. 4). The optimum geometry combination is determined by using the optimal values for each parameter. For the most efficient optimum design (OD), the length of the flow straightener, rotor and diffuser blades are 5 mm, 10 mm and 10 mm respectively, while the wrap angles of the straightener, rotor and diffuser blades are 160, 360 and 10 degrees respectively. The results indicate that the pump efficiency increases when the wrap angles of the blades are increased. In order to maximise efficiency, additional geometries were constructed by increasing the wrap angles further.

Additional optimisation was conducted by adjusting the length of the rotor at the centre in relation to its length at the tip. The results showed that increasing the length of the rotating blade near the centreline to 18 mm while maintaining a tip length of 10 mm led to an increase in the pump head and efficiency, as listed in Table 2a. Incorporating these parameters into the optimisation process resulted in an improved optimal design (IOD). The computational predictions for this additional geometry show that the desired pump performance is achieved by providing a 5 L/min mass flow rate together with a 40 mmHg pressure rise at 2900 rpm, with additional improvements in efficiency and outlet pressure. Thus, the optimal geometry of the pump has a rotor that is longer at the centre, and the wrap angles of the flow straightener and diffuser blades are 35 and 260 degrees respectively.

3.2. CFD results

Computational predictions show that the new intra-aortic pump is able to generate 5 L/min flow rate over 40 mmHg pressure rise for 2900 RPM. Fig. 5 shows the streamline formation from the velocity vectors

Table 2
(a) OD and IOD parameters and values, and (b) CFD performance results of OD and IOD values of the Intra-aortic pump design.

(a)

Optimization Parameters	Values of parameters for OD	Values of parameters for IOD
length of straightener blades (mm)	5	5
length of rotor blades at the shroud (mm)	10	10
length of rotor blades at the center (mm)	**10**	**18**
length of diffuser blades (mm)	10	10
wrap angle of rotor (degree)	360°	360°
wrap angle of diffuser (degree)	160°	160°
inlet angle of rotor (degree)	1°	1°
inlet angle of diffuser (degree)	1°	1°
outlet angle of rotor (degree)	2°	2°
inlet angle of straightener (degree)	10°	10°
Distance between rotor and straightener (mm)	3	3
Distance between rotor and diffuser (mm)	1	1

(b)

	Pressure rise (mmHg)	Moment (Nm)	Rotor speed (rpm)	Shaft power (W)	Hydraulic power (W)	Efficiency
OD	26.26	0.00487	2900	1.480	0.203	13.75%
IOD	43.6	0.00787	2900	2.389	0.338	14.14%

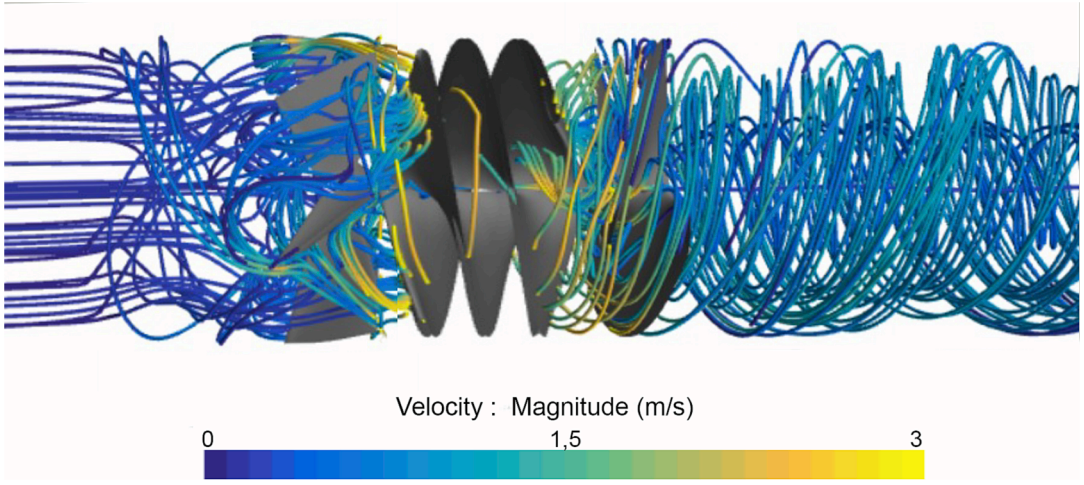

Fig. 5. Velocity distribution of fluid domain.

starting at both the inlet and exit planes. The figure illustrates the contribution of the straightener in guiding the flow to the rotor blades in order to maximize momentum change as the flow interacts with the rotor. The figure also demonstrates the complexity of the flow around the rotor blades. The spatial distribution of the shear stress on the blade surfaces for the improved optimum design (IOD) is shown in Fig. 6. Wall shear stress is acting tangentially at the interface between the fluid blood and the solid surface of the pump blades. Wall shear stress can lead to deformation and breakage of red blood cells. It can be seen from Fig. 6 that the highest wall shear stress is located by the middle of the rotor closest to the diffuser.

The final results from the CFD model are summarised in Table 2b. It shows that the hydraulic efficiency for the optimum design (OD) is about 13% but it is not able to achieve the required pressure rise of 40 mmHg at 2900 rpm. With the IOD the pump efficiency is slightly increased to 14 %, with a significant increase in the pressure rise to 43.6 mmHg at the same rotational, speed 2900 rpm.

Based on Garon et al. (2004), who modelled hemolysis by solving a Hyperbolic Partial Differential Equation within the frame of an Euler approach, the hemolysis indices are calculated using CFD for the IOD. The modified index of hemolysis (MIH) value is found to be only 36, which falls well below the calculated values for other LVADs, typically exceeding 1000 (Thamsen et al., 2015; Garon and Farinas, 2004). The

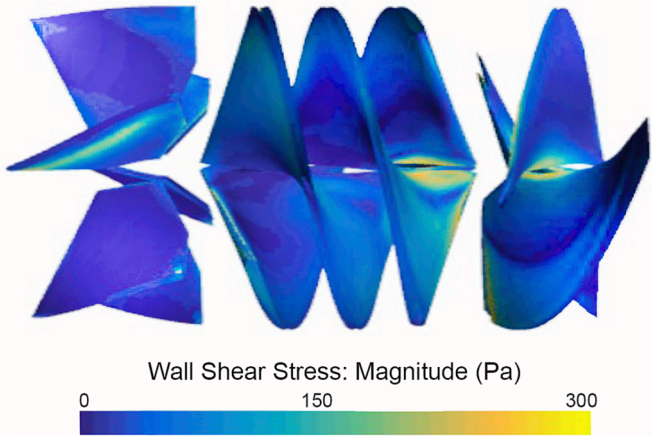

Fig. 6. WSS distribution on blade surfaces.

low value can be attributed to the low rpm (2900 rpm) compared to more than 8000 rpm for other pumps. Another reason is that the proposed pump is not required to raise the pressure to 120 mm Hg as it works in series with heart and therefore the shear forces and the exposed

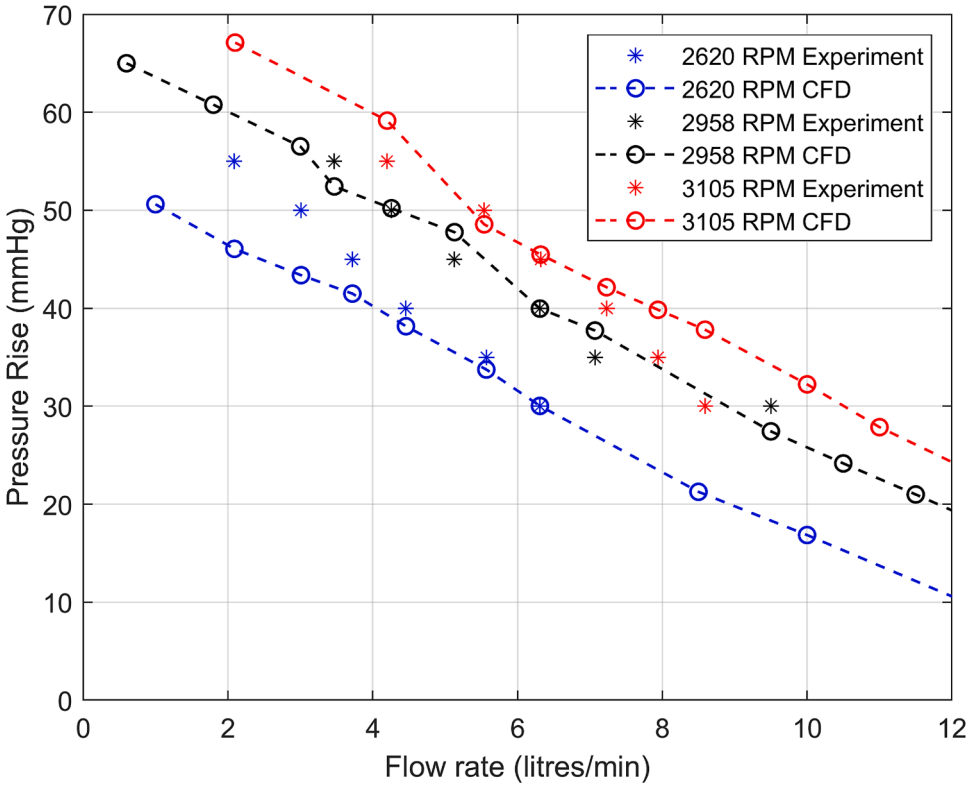

Fig. 7. The pump performance in comparison with the experimental and CFD simulations results.

time for such shear forces are much lower. This is the main advantage of having the pump located in the aorta.

3.3. Experimental results

Fig. 7 compares experimental results and CFD predictions for the performance of the IOD prototype. Experimentally, the pressure rise of the pump prototype was found to be slightly higher than the CFD predictions for 2620 RPM rotational speed while it is a little lower for 3105 RPM. The prototype performance met the design requirements of mass flow rate and pressure generation at lower rotational speeds. The pump performance curve is extended using the CFD model, as illustrated in Fig. 7. In vivo, the pump is designed to operate with a flow rate exceeding 3 L/min, depending on the individual's activity level (Hall, 1999; Guyton, 1973). To obtain the total torque required for operating the pump, the torque resulting from the pressure and shear stress distribution over the rotor surface was integrated. Subsequently, the shaft power and efficiency were computed. The pump's efficiency consistently remains around 14% within the simulated flow rate range. This is attributed to the increase in torque as the pump flow rate rises. The pump power increased with the pump flow rate resembles that of the HeartMate 2 axial pump, as demonstrated by (Asgari and Bonde, 2014).

The heart generates a pulsatile flow; the intra-aortic pump, working in series, will provide additional pressure in sync with the cardiac cycle. The flow rate of the system depends on the ECG signal which varies depending on the person's activity. A control system (to be developed) will change the pump rpm based on the ECG signal.

4. Discussion

Experimental results have verified that the proposed VAD can deliver the required pump performance with a reduction of rotational speed by a factor of three or more. Thus, the axial LVADs use between 9000 and 18000 rpm to provide the performance that the intra-aortic LVAD delivers at 2900 rpm. This is possible because for a fixed mass flow rate, the flow velocity is inversely proportional to the flow area, and the intra-aortic placement allows the LVAD to have an almost three times larger flow diameter. Decreasing the rotation speed is in turn highly effective in reducing WSS, and hence reducing hemolysis risk.

Various parameters have been optimised for the shaftless pump design, and the general dimensions of the device were defined after the design optimisation study. The length of the new design is about 3 cm and the total weight is around 60 g. Thus, the intro-aortic LVAD is small and lighter than the other LVADs (500 gr Heartmate-3; 79 gr Heartware-MVAD). Given that there is no need for artificial vessels to bypass, the blood contact surface area decreases significantly. In addition, the surgical operation time and risk are reduced by using minimally invasive implantation techniques for intra-aortic placement. Thus, only a small cut on the aorta is enough for implementation, and there is no need for any cut in the heart itself. The Outcome of this work is in line with recent developments which focus on miniaturisation and the development of surgical minimally invasive procedures for LVAD to overcome possible complications such as infections, major incisions, right heart failure and bleeding events (Chatterjee et al., 2020; Starling et al., 2014). The proposed new LVAD could assist in reducing hospital stays and overall treatment expenses. Since there is no cut on the heart, bleeding events are less likely to occur. Accordingly, the need for transfusions is reduced, along with the risk of infections.

The results highlight that the energy consumption of the new device is dramatically lower than the LVADs in use even though it has lower hydraulic efficiency. High energy consumption of the LVADs, which makes wireless energy transfer insufficient, is another underlying reason for complications. Miller states that although there are numerous recent technological advancements in the development of LVADs, none of them is more significant than transforming to wireless power (Miller, 2018). When the power is transmitted into the body with a cable, this raises the possibility of device-related infections, which are one of the main causes of patient death. The low energy consumption (<3 W) of the intra-aortic LVAD allows for wireless energy transfer, which minimises the risk of device-related infection. However, the hydraulic efficiency of the new

LVAD is about 14%, while it reaches almost 30% for other axial LVADs. The evaluation of the CFD path lines shows that the turbulence is higher at the centre. Thus, the hubless blade design is the main reason for lower efficiency. On the other hand, a hubless blade design is essential for intra-aortic placement because there should be no high resistance behind blood flow when the device stops suddenly. Considering that the energy consumption is suitable for wireless energy transfer and it has advantages that will increase the life quality and lifespan of the patients by reducing side effects, it is less important that the hydraulic efficiency is lower than other devices. It is likely that further efficiency improvements will emerge with additional optimisation studies.

As the aim of this study has been to optimise the pump blades to achieve the required flow and head with minimum power, we have only considered a steady flow condition. This is a valid approach assuming the pulsatile flow cycle is long enough to be represented by a series of quasi-steady processes. This assumption has been adopted by many authors when optimising LVAD rotors (Antony et al., 2021; Fraser et al., 2012). However, detailed analysis of unsteady flow behaviour will be required to develop the corresponding control system to operate in support of the patient's cardiac cycle.

CRediT authorship contribution statement

Elif Oran: Writing- Review & Editing, Methodology, Investigation, Validation, Software, Supervision, Visualisation, Formal Analysis, Funding acquisition. **Essam Abo-Serie:** . **James Jewkes:** Writing – review & editing, Validation, Supervision, Software, Methodology. **Manus Henry:** Writing – review & editing, Validation, Supervision, Project administration, Methodology, Investigation. **Bulent Oran:** Writing – review & editing, Visualization, Supervision, Project administration, Methodology, Investigation, Conceptualization.

Declaration of Competing Interest

The authors declare that they have no known competing financial interests or personal relationships that could have appeared to influence the work reported in this paper.

Acknowledgments

The authors would like to acknowledge the financial support provided by Coventry University UK, University of Leicester UK and Misal Limited Company. The author would also like to acknowledge the software support provided by CFturbo.

References

Abo-Serie, E., Oran, E., Oran, B., & Cirstea, R. (2018). Analysis of Intra-Aortic Axial Pump for Heart Assist, SIMBIO-M Conference, Stratford-Upon-Avon, UK.

Al-Naamani, Ameen, et al. (2021). Minimally invasive ventricular assist device implantation. Journal of thoracic disease 13.3 (2021): 2010.

Antony, M., Rajasiva, L.M., Tomy, J., Roy, P.P., Yadu, P.V., 2021. Design, analysis and validation axial ventricular assist device. Mater. Today:. Proc. 47, 5313–5318.

Asgari, S.S., Bonde, P., 2014. Implantable physiologic controller for left ventricular assist devices with telemetry capability. J. Thorac. Cardiovasc. Surg. 147 (1), 192–202.

Behbahani, M., Behr, M., Hormes, M., Steinseifer, U., Arora, D., Coronado, O., Pasquali, M., 2009. A review of computational fluid dynamics analysis of blood pumps. Eur. J. Appl. Math. 20 (4), 363–397.

Benjamin, Emelia J., et al. (2017). Heart disease and stroke statistics 2017 update: a report from the American Heart Association. Circulation 135.10 (2017): e146-e603.

Boyle, Andrew J., et al. (2014). Pre-operative risk factors of bleeding and stroke during left ventricular assist device support: an analysis of more than 900 HeartMate II outpatients. J. Am. College Cardiol. 63.9 (2014): 880-888.

Burggren, W.W., et al., 2014. Comparative cardiovascular physiology: future trends, opportunities and challenges. Acta Physiol. 210 (2), 257–276.

Califano, S., Pagani, F.D., Malani, P.N., 2012. Left ventricular assist device–associated infections. Infect. Dis. Clin. 26 (1), 77–87.

Carrozzini, M., Bejko, J., Gerosa, G., Bottio, T., 2019. Bilateral mini-thoracotomy approach for minimally invasive implantation of HeartMate 3. Artif. Organs 43 (6), 593–595.

Chaichana, T., Sun, Z., Jewkes, J., 2011. Computation of hemodynamics in the left coronary artery with variable angulations. J. Biomech. 44 (10), 1869–1878.

Chatterjee, Anamika, et al. (2020). Minimally invasive left ventricular assist device implantation: optimizing device design for this approach. Expert Rev. Med. Devices 17.4 (2020): 323-330.

Chen, Z., Jena, S.K., Giridharan, G.A., Koenig, S.C., Slaughter, M.S., Griffith, B.P., Wu, Z. J., 2018. Flow features and device-induced blood trauma in CF-VADs under a pulsatile blood flow condition: a CFD comparative study. Int. J. Numer. Methods Biomed. Eng. 34 (2), e2924.

Cheng, L., Tan, J., Yun, Z., Wang, S., Yu, Z., 2021. Analysis of flow field and hemolysis index in axial flow blood pump by computational fluid dynamics–discrete element method. Int. J. Artif. Organs 44 (1), 46–54.

Dewi, D.E.O., Yusof, N.S.M., 2020. Tissue-mimicking materials for cardiac imaging phantom—section 1: from conception to materials selection. Cardiovas. Eng.: Technol. Advancements, Rev., Appl. 3–33.

Fang, James C., et al. (2015). Advanced (stage D) heart failure: a statement from the Heart Failure Society of America Guidelines Committee. J. Cardiac Failure 21.6 (2015): 519-534.

Fraser, K.H., Taskin, M.E., Griffith, B.P., Wu, Z.J., 2011. The use of computational fluid dynamics in the development of ventricular assist devices. Med. Eng. Phys. 33 (3), 263–280.

Fraser, Katharine H., et al. (2012). A quantitative comparison of mechanical blood damage parameters in rotary ventricular assist devices: shear stress, exposure time and hemolysis index. (2012): 081002.

Fuchs, M., Schibilsky, D., Zeh, W., Berchtold-Herz, M., Beyersdorf, F., Siepe, M., 2019. Does the heart transplant have a future? Eur. J. Cardiothorac. Surg. 55 (Supplement_1), i38–i48.

Gamechi, Z., Zahra, et al., 2019. Automated 3D segmentation and diameter measurement of the thoracic aorta on non-contrast enhanced CT. Eur. Radiol. 29, 4613–4623.

Garon, A., Farinas, M.I., 2004. Fast three-dimensional numerical hemolysis approximation. Artif. Organs 28 (11), 1016–1025.

Guyton, A.C. (1973). Cardiac output and its regulation, W.B. Saunders Company; 2nd edition (12 Jun. 1973) 353-371.

Hall, J.E., 1999. Integration and regulation of cardiovascular function. Adv. Physiol. Educ. 277 (6), S174.

Kälsch, H., Lehmann, N., Möhlenkamp, S., et al., 2013. Body-surface adjusted aortic reference diameters for improved identification of patients with thoracic aortic aneurysms: results from the population-based Heinz Nixdorf Recall study. Int. J. Cardiol. 163, 72–78.

Khoo, D.P., Cookson, A.N., Gill, H.S., Fraser, K.H., 2018. Normal fluid stresses are prevalent in rotary ventricular assist devices: A computational fluid dynamics analysis. Int. J. Artif. Organs 41 (11), 738–751.

Kirklin, J.K., Naftel, D.C., Kormos, R.L., Pagani, F.D., Myers, S.L., Stevenson, L.W., Miller, M.A., 2014. Interagency Registry for Mechanically Assisted Circulatory Support (INTERMACS) analysis of pump thrombosis in the HeartMate II left ventricular assist device. J. Heart Lung Transplant. 33 (1), 12–22.

McElroy, M., Xenakis, A., Keshmiri, A., 2020. Impact of heart failure severity on ventricular assist device haemodynamics: a computational study. Res. Biomed. Eng. 36, 489–500.

Mehra, M.R., Goldstein, D.J., Uriel, N., Cleveland Jr, J.C., Yuzefpolskaya, M., Salerno, Naka, Y., 2018. Two-year outcomes with a magnetically levitated cardiac pump in heart failure. N. Engl. J. Med. 378 (15), 1386–1395.

Messer, S., Page, A., Rushton, S., Berman, M., Tsui, S., Catarino, P., Large, S.R., 2019. The potential of heart transplantation from donation after circulatory death donors within the United Kingdom. J. Heart Lung Transplant. 38 (8), 872–874.

Miller, L.W., Rogers, J.G., 2018. Evolution of left ventricular assist device therapy for advanced heart failure: a review. JAMA Cardiol. 3 (7), 650–658.

Mori, S., Tretter, J.T., Spicer, D.E., Bolender, D.L., Anderson, R.H., 2019. What is the real cardiac anatomy? Clin. Anat. 32 (3), 288–309.

Nammakie, E., Niroomand-Oscuii, H., Koochaki, M., Ghalichi, F., 2017. Computational fluid dynamics-based study of possibility of generating pulsatile blood flow via a continuous-flow VAD. Med. Biol. Eng. Compu. 55, 167–178.

Nassif, M.E., LaRue, S.J., Raymer, D.S., Novak, E., Vader, J.M., Ewald, G.A., Gage, B.F., 2016. Relationship between anticoagulation intensity and thrombotic or bleeding outcomes among outpatients with continuous-flow left ventricular assist devices. Circulat. Heart Failure 9 (5), e002680.

Netuka, Ivan, et al. (2017). Outcomes in HeartMate II patients with no antiplatelet therapy: 2-year results from the European TRACE Study. The Annals Thoracic Surg. 103.4 (2017): 1262-1268.

Oran B., Oran E., (2017). Endovascular permanent heart assist device. 2017, US Patent 9,555,175.

Parameshwar, J., et al., 2019. Patient survival and therapeutic outcome in the UK Bridge to transplant left ventricular assist device population. Heart 105 (4), 291–296.

Puhan, P., Awasthi, A., Mukherjee, A.K., Atta, A., 2021. CFD modeling of segregation in binary solid-liquid fluidized beds: Influence of liquid viscosity and density. Chem. Eng. Sci. 246, 116965.

Ribaric, S., Kordaš, M., 2011. Teaching cardiovascular physiology with equivalent electronic circuits in a practically oriented teaching module. Adv. Physiol. Educ. 35 (2), 149–160.

Rogers, J.G., Bostic, R.R., Tong, K.B., Adamson, R., Russo, M., Slaughter, M.S., 2012. Cost-effectiveness analysis of continuous-flow left ventricular assist devices as destination therapy. Circulat. Heart Failure 5 (1), 10–16.

Sarkisyan, H., Stevens, R., Tchantchaleishvili, V., Rossano, J., Throckmorton, A., 2021. Integrated long-term multifunctional pediatric mechanical circulatory assist device. Artif. Organs 45 (5), E65–E78.

Silva, P.A., Tsoutsanis, P., Antoniadis, A.F., 2021. Simple multiple reference frame for high-order solution of hovering rotors with and without ground effect. Aerosp. Sci. Technol. 111, 106518.

Singh, V.R., Zinzuvadia, M.J., Sheth, S.M., 2017. Parametric study and design optimization of centrifugal pump impeller-a review. Int J Eng Res Appl. Kalpa Publicat. Eng. 1, 507–515.

Slaughter, Mark S., et al. (2010). Post-operative heparin may not be required for transitioning patients with a HeartMate II left ventricular assist system to long-term warfarin therapy. J. Heart Lung Transplant. 29.6 (2010): 616-624.

Smith, P.A., Wang, Y., Metcalfe, R.W., Sampaio, L.C., Timms, D.L., Cohn, W.E., Frazier, O.H., 2018. Preliminary design of the internal geometry in a minimally invasive left ventricular assist device under pulsatile-flow conditions. Int. J. Artif. Organs 41 (3), 144–151.

Starling, Randall C., et al. (2011), Results of the post-US Food and Drug Administration-approval study with a continuous flow left ventricular assist device as a bridge to heart transplantation: a prospective study using the INTERMACS (Interagency Registry for Mechanically Assisted Circulatory Support). J. Am. College Cardiol. 57.19 (2011): 1890-1898.

Starling, R.C., Moazami, N., Silvestry, S.C., et al., 2014. (2014) Unexpected abrupt increase in left ventricular assist device thrombosis. N Engl J Med 370, 33–40.

Stawiarski, K., Ramakrishna, H., 2021. Left ventricular mechanical circulatory support—assessing outcomes with new data. J. Cardiothor. Vascular Anesthesia 35 (ISSN 2499–2502), 1053.

Thamsen, B., Blümel, B., Schaller, J., Paschereit, C.O., Affeld, K., Goubergrits, L., Kertzscher, U., 2015. Numerical analysis of blood damage potential of the HeartMate II and HeartWare HVAD rotary blood pumps. Artif. Organs 39 (8), 651–659.

Topkara, V.K., et al., 2016. Myocardial recovery in patients receiving contemporary left ventricular assist devices: results from the Interagency Registry for Mechanically Assisted Circulatory Support (INTERMACS). Circulat. Heart Failure 9 (7), e003157.

Vasudevan, V.S., Simaan, M.A., Maul, T.M., Wearden, P.D., 2019. Aortic Valve Ejection Fraction for Monitoring Heart Contractility in Patients Supported with a Continuous Flow Left Ventricular Assist Device. Am. J. Cardiovasc. Thoracic Surg. 4 (2).

Vignali, E., Gasparotti, E., Mariotti, A., Haxhiademi, D., Ait-Ali, L., Celi, S., 2022. High-versatility left ventricle pump and aortic mock circulatory loop development for patient-specific hemodynamic in vitro analysis. ASAIO J. 68 (10), 1272–1281.

Wilcox, D.C. (1998). Turbulence modeling for CFD (Vol. 2, pp. 103-217). La Canada, CA: DCW industries.

Wolak, A., et al., 2008. Aortic size assessment by noncontrast cardiac computed tomography: normal limits by age, gender, and body surface area. J. Am. Coll. Cardiol. Img. 1 (2), 200–209.

Zhou, L., Shi, W., Wu, S., 2013. Performance optimization in a centrifugal pump impeller by orthogonal experiment and numerical simulation. Adv. Mech. Eng. 5, 385809.